Size dependent analysis of tapered FG micro-bridge based on a 3D beam theory

S. Haddad[a], M. Baghani[b,1], M.R. Zakerzadeh[c]

School of Mechanical Engineering, College of Engineering, University of Tehran, Tehran, Iran.

[a] School of Mechanical Engineering, College of Engineering, University of Tehran, Tehran, Iran, s.haddad@ut.ac.ir

[b] School of Mechanical Engineering, College of Engineering, University of Tehran, Tehran, Iran, baghani@ut.ac.ir

[c] School of Mechanical Engineering, College of Engineering, University of Tehran, Tehran, Iran, zakerzadeh@ut.ac.ir

Abstract

In the current study, an analytical solution based on modified couple stress theory for a nonlinear model describing the couple 3D motion of a functionally graded tapered micro-bridge is presented. The small scale effects and the nonlinearity arising from the mid-plane stretching are taken into consideration. Governing equations of motions are derived utilizing modified couple stress theory and applying Hamilton principle. Dynamic and static analysis to determine the effects of lateral distributed forces and mid-plane stretching are investigated. To this aim, analytical Homotopy-pade technique is employed to capture the nonlinear natural frequencies in high amplitude vibrations of tapered micro-bridges with different types of geometries and material compositions. The obtained results of frequencies propose that there is a good agreement between the present analytical results and the numerical ones in opposed to well-known multiple-scale method. Furthermore, comparing the results in 2D and 3D analysis shows that in 2D analysis, the stiffness and natural frequency of the micro-beam is underestimated and we observe that increasing the tapered ratio has different impacts on natural frequencies for micro-beams with different slender ratios.

Keywords: Micro-bridge, 3D beam theory, Modified couple stress, Tapered beam, Analytical HAM solution.

1 Introduction

Micro-beams have a major importance in the fields of micro/nono electro-mechanical systems such as those in sensors and actuators [1].Beams used in these applications have the thickness in order of microns and sub-microns. The size dependent behavior of these structures has been empirically observed by several researchers [2–5]. Incorporating the concept of length scale parameter, an experimentally measurable property accounting for dislocation and distortion of constitutive crystals and grain size of a specific material [6] have led to many investigations on size effect phenomena during past few decades and some non-classical continuum theories have been developed. Mindlin [7] introduced higher-order gradient theory, regarding the first and the second derivatives of the strain tensor, for elastic materials. after that, using Mindlin's formulation, the strain gradient theory was proposed by Fleck & Hutchinson [8–10] which considers only the first derivatives of the strain tensor. Ansari [11] developed a model using modified strain gradient theory to describe the linear and nonlinear vibrational behavior of a fractional viscoelastic Timoshenko micro/nano beams. In this paper, predictor–corrector technique is utilize to deal with the set of nonlinear governing equations. Based on strain gradient elasticity theory, an analytical solution is proposed for an Euler-Bernoulli FG nano beam by Li et al. [12]. In this study, the device is lying on an elastic foundation and the bending and buckling behavior are investigated.

[1] Corresponding author email address: baghani@ut.ac.ir, tel.: +982161119921

Another well-known theory which involves size effects, is the couple stress theory introduced by Mindlin & Tiersten[13].

The modified couple stress theory proposed by Yang et al, [6] considers the equilibrium equation of forces and couples and moments of couples applied to a single material element. In this theory, two classical and one additional material constants are introduced to reflect the microstructure-related size influences.

Based on the modified couple stress theory, the dynamic and static response of homogeneous and functionally graded materials, including linear vibration, elastic bending, post buckling and non-linear vibration have been investigated by many researchers[14–17]. Functionally graded materials (FGMs) are inhomogeneous composites of two different constituents, typically a metal and a ceramic, with a desired continuous change in compositional characteristics as a function of position along specified dimensions. Application of FGMs has been widely extended in various industrial fields specially in designing Micro and Nano systems such as thin films in the form of shape memory alloys [18,19] atomic force microscopes (AFMs) [20], also Micro/Nano electro-mechanical systems [21–25]

In addition to FG functionality in micro beams, Non-prismatic beams, i.e. beams with a varying cross-section (abruptly or gradually) along the length of the beam, play an important role in different fields [26] in which they can be used in the architectural and aesthetic aspects of engineering design to optimize the strength and weight of the structure. One of the effective application of tapered micro beams is in micro energy harvester in which tailoring the structural parameters of the cantilever beam could lead to an increased harvester power [27] and can considerably influence the natural frequency of microstructures [28]. Baghani et al, [26] by considering the assumption of inextensibility of neutral axis, studied large amplitude free vibrations of tapered micro-bridges on a nonlinear elastic foundation. Dynamic analysis of a parabolic tapered Euler–Bernoulli cantilever beam under a travelling mass is accomplished by Zhao et al. [29].

In most of the investigations performed on the behavior of micro and sub micro beams, the problem is considered as a 2D case, so there is a geometric imperfection, since the beam is under 3D deformation and the-mid plane stretching may lead to a coupling between the displacements of lateral directions. Due to the importance of micro-beams and micro-systems, the couple 3D deformations of these structures have been studied by many researchers. Considering mid plane stretching and geometric non-linearity, Mojahedi, Ahmadian et al. [30,31], and Mojahedi & Rahaeifard [32] studied the 3 Dimensional motion for the micro/Nano beam and reported the static, dynamic and instability behavior of electro-static actuated bridge and cantilever micro/Nano gyroscope and micro bridges.

The Euler Bernoulli beam theory is the most well-known theory for calculating beam deformation with the slender ratio, commonly $L/h>10$. According to this theory, due to ignoring shear strains, a plane after deformation remain plane and still perpendicular to the central line of the beam. Employing the modified couple stress theory in Euler-Bernoulli beam model, the results show a larger bending stiffness than the classical ones [33]. Euler-Bernoulli beam theory can predict the lateral and bending deformation. However, in this paper, strain tensor is built to include the deformation in both lateral and in axial directions.

The aim of is this paper, at first is to present a mechanical model to illustrate the 3D motion of an FGM double tapered micro-bridge, afterwards, the impacts of nonlinearity caused by considering the third dimension into the calculations and the effects of material composition, tapered ratio and geometrical properties on the static and dynamic responses are investigated. An analytical Homotopy –pade method is implemented to estimate the natural frequencies of the micro-bridges. As it will be discussed in the paper, the Homotopy method is more general than multiple scale methods employed in many nonlinear problems [34]. In multiple time scale (MTS) technique, using a small physical parameter, the nonlinear problems is transferred into a sequence of linear perturbed problems while this small parameter is not needed in HAM and gaining higher –order approximation are easier, leading to smaller computational cost. In addition to low simulation cost, here we demonstrate that HAM is more appropriate for strong nonlinearities and high amplitudes. For this purpose, a comparison study is accomplished to capture the

accuracy of HAM as opposed to MTS, as a classic perturbation method. The consistency of the calculated analytical results with the numerical ones are also presented.

2 Problem formulation

Fig. (1) shows two views of FG tapered micro-bridge under lateral loads. The deformation and distributed load in z direction are depicted by $\hat{w}\left(\hat{x},\hat{t}\right)$, $\hat{f_z}$, and in y direction by $\hat{v}(\hat{x},\hat{t})$ and $\hat{f_y}$, respectively. The strain energy density, employing the couple stress theory, is written as:

$$\tilde{\upsilon}=\frac{1}{2}\left(\sigma_{ij}\varepsilon_{ij}+\chi_{ij}m_{ij}\right) \tag{1}$$

Where σ_{ij} and ε_{ij} are the components of stress and strain tensor, respectively, m_{ij} is the deviatoric part of the couple stress tensor and χ_{ij} is the symmetric curvature tensor.

Assuming flexible motions in both directions, the relation between transverse displacements and the rotation vector components becomes:

$$\vec{\theta}=-\frac{\partial\hat{w}}{\partial\hat{x}}\hat{e}_2-\frac{\partial\hat{v}}{\partial\hat{x}}\hat{e}_3 \tag{2}$$

The non-zero components of the deviatoric part of the couple stress tensor and the symmetric curvature tensor are recorded as:

$$\begin{cases}\chi_{ij}=\frac{1}{2}\left(\theta_{i,j}+\theta_{j,i}\right)\\ m_{ij}=2l^2\mu\chi_{ij}\end{cases}\rightarrow\begin{cases}m_{xy}=m_{yx}=-\mu l^2\frac{\partial^2\hat{w}}{\partial\hat{x}^2}\\ m_{xz}=m_{zx}=-\mu l^2\frac{\partial^2\hat{v}}{\partial\hat{x}^2}\end{cases} \tag{3}$$

In which l and μ symbolize the material length scale parameter and the shear modulus, respectively. The displacement filed according to Euler-Bernoulli beam theory for a micro-beam subjected to distributed load in both lateral directions can be written as[35]:

$$u_1=\hat{u}-\hat{z}\frac{\partial\hat{w}}{\partial\hat{x}}-\hat{y}\frac{\partial\hat{v}}{\partial\hat{x}}\qquad u_2=\hat{v}\left(\hat{x}\right),\quad u_3=\hat{w}\left(\hat{x}\right) \tag{4}$$

Where $\hat{u}$ is the axial deformation. Utilizing the von-Karman relation, the nonzero strain (i.e. the axial strain) is derived [32]:

$$\varepsilon_x=\frac{\partial\hat{u}}{\partial\hat{x}}-\hat{z}\frac{\partial^2\hat{w}}{\partial\hat{x}^2}-\hat{y}\frac{\partial^2\hat{v}}{\partial\hat{x}^2}+\frac{1}{2}\left(\frac{\partial\hat{v}}{\partial\hat{x}}\right)^2+\frac{1}{2}\left(\frac{\partial\hat{w}}{\partial\hat{x}}\right)^2 \tag{5}$$

Thus, the axial stress in the beam would be

$$\sigma_x=E\left[\frac{\partial\hat{u}}{\partial\hat{x}}-\hat{z}\frac{\partial^2\hat{w}}{\partial\hat{x}^2}-\hat{y}\frac{\partial^2\hat{v}}{\partial\hat{x}^2}+\frac{1}{2}\left(\frac{\partial\hat{v}}{\partial\hat{x}}\right)^2+\frac{1}{2}\left(\frac{\partial\hat{w}}{\partial\hat{x}}\right)^2\right] \tag{6}$$

In which E is the young modulus of elasticity.

The potential and kinetic energy of the beam according to Equation (1) is written, respectively as:

$$V=\int_0^L \left[\iint_A \tilde{\upsilon} dA \right] d\hat{x} =$$

$$\frac{1}{2}\int_0^L \left[\iint_A \left(\sigma_x \varepsilon_x + \chi_{xy} m_{xy} + \chi_{yx} m_{yx} + \chi_{xz} m_{xz} + \chi_{zx} m_{zx} \right) dA \right] d\hat{x} \tag{7}$$

$$T = \frac{1}{2}\int_0^L \rho(\hat{x}) A(\hat{x}) \left[\left(\frac{\partial \hat{u}}{\partial \hat{t}} \right)^2 + \left(\frac{\partial \hat{v}}{\partial \hat{t}} \right)^2 + \left(\frac{\partial \hat{w}}{\partial \hat{t}} \right)^2 \right] d\hat{x} \tag{8}$$

where $\rho(\hat{x})$, $A(\hat{x})$ and L are the mass per unit volume, cross section and the length of the beam respectively. The work of external forces on the micro bridge is structured in the form of:

Considering the work of external forces on the micro bridge as $W_{ext} = \int_0^L \left[\hat{f}_y \hat{v} + \hat{f}_z \hat{w} \right] d\hat{x}$, the Lagrangian of the motion, then is given as:

$$L = T - V + W_{ext}$$

$$= \frac{1}{2}\int_0^L \rho(\hat{x}) A(\hat{x}) \left[\left(\frac{\partial \hat{u}}{\partial \hat{t}} \right)^2 + \left(\frac{\partial \hat{v}}{\partial \hat{t}} \right)^2 + \left(\frac{\partial \hat{w}}{\partial \hat{t}} \right)^2 \right] d\hat{x} -$$

$$\int_A E(\hat{x}) \begin{bmatrix} \left(\frac{\partial \hat{u}}{\partial \hat{x}} - \hat{z} \frac{\partial^2 \hat{w}}{\partial \hat{x}^2} - y \frac{\partial^2 \hat{v}}{\partial \hat{x}^2} + \frac{1}{2}\left(\frac{\partial \hat{v}}{\partial \hat{x}} \right)^2 + \frac{1}{2}\left(\frac{\partial \hat{w}}{\partial \hat{x}} \right)^2 \right)^2 \\ -\mu(\hat{x}) l(\hat{x})^2 \left(\frac{\partial^2 \hat{v}}{\partial \hat{x}^2} \right)^2 - \mu(\hat{x}) l(\hat{x})^2 \left(\frac{\partial^2 \hat{w}}{\partial \hat{x}^2} \right)^2 \end{bmatrix} d\hat{x} + \int_0^L \left[\hat{f}_y \hat{v} + \hat{f}_z \hat{w} \right] d\hat{x} \tag{9}$$

Applying the Hamilton principle, we have:

$$\delta \int_0^{\hat{t}} L \, d\hat{t} = 0 \tag{10}$$

Expanding the integral in Equation (10), governing equations of motion for the doubly clamped micro-beam are as follows:

$$\frac{\partial}{\partial \hat{x}} \left(\mathrm{E}(\hat{x}) \mathrm{A}(\hat{x}) \left(\frac{\partial \hat{u}}{\partial \hat{x}} + \frac{1}{2}\left(\frac{\partial \hat{v}}{\partial \hat{x}} \right)^2 + \frac{1}{2}\left(\frac{\partial \hat{w}}{\partial \hat{x}} \right)^2 \right) \right) = \rho(\hat{x}) A(\hat{x}) \frac{\partial^2 \hat{u}}{\partial \hat{\mathrm{t}}^2} \tag{11}$$

$$\rho(\hat{x}) A(\hat{x}) \frac{\partial^2 \hat{v}}{\partial \hat{t}^2} + \frac{\partial^2}{\partial \hat{x}^2} \left(\left(\mu(\hat{x}) A(\hat{x}) l(\hat{x})^2 + E(\hat{x}) I_z(\hat{x}) \right) \frac{\partial^2 \hat{v}}{\partial \hat{x}^2} \right) -$$

$$\frac{\partial}{\partial \hat{x}} \left(E(\hat{x}) A(\hat{x}) \left(\frac{\partial \hat{u}}{\partial \hat{x}} + \frac{1}{2}\left(\frac{\partial \hat{v}}{\partial \hat{x}} \right)^2 + \frac{1}{2}\left(\frac{\partial \hat{w}}{\partial \hat{x}} \right)^2 \right) \frac{\partial \hat{v}}{\partial \hat{x}} \right) = \hat{f}_y \tag{12}$$

$$\rho(\hat{x})A(\hat{x})\frac{\partial^2\hat{w}}{\partial\hat{t}^2}+\frac{\partial^2}{\partial\hat{x}^2}\left(\left(\mu(\hat{x})A(\hat{x})l(\hat{x})^2+E(\hat{x})I_y(\hat{x})\right)\frac{\partial^2\hat{w}}{\partial\hat{x}^2}\right)-$$
$$\frac{\partial}{\partial\hat{x}}\left(E(\hat{x})A(\hat{x})\left(\frac{\partial\hat{u}}{\partial\hat{x}}+\frac{1}{2}\left(\frac{\partial\hat{v}}{\partial\hat{x}}\right)^2+\frac{1}{2}\left(\frac{\partial\hat{w}}{\partial\hat{x}}\right)^2\right)\frac{\partial\hat{w}}{\partial\hat{x}}\right)=\hat{f}_z \quad (13)$$

In Equation (14), the appropriate boundary conditions are given for the doubly clamped microbridge.

$$\hat{u}(0,\hat{t})=\hat{u}(\hat{L},\hat{t})=0,\qquad \hat{v}(0,\hat{t})=\hat{v}(\hat{L},\hat{t})=0,\quad \frac{\partial\hat{v}}{\partial\hat{x}}(0,\hat{t})=\frac{\partial\hat{v}}{\partial\hat{x}}(\hat{L},\hat{t})=0$$
$$\hat{w}(0,\hat{t})=0,\ \hat{w}(L,\hat{t})=0,\quad \frac{\partial\hat{w}}{\partial\hat{x}}(0,\hat{t})=0,\ \frac{\partial\hat{w}}{\partial\hat{x}}(L,\hat{t})=0 \quad (14)$$

In the case of no axial forces, longitudinal inertia is negligible [31], thus, by solving Equation (11) and applying the corresponding boundary conditions, we arrive at:

For doubly clamped BCs:

$$u_{bridge}(\hat{x},\hat{t})=-\int_0^{\hat{x}}\left[\frac{1}{2}\left(\frac{\partial\hat{v}}{\partial\hat{x}}\right)^2+\frac{1}{2}\left(\frac{\partial\hat{w}}{\partial\hat{x}}\right)^2\right]d\hat{x}\ +\frac{\int_0^{\hat{x}}\frac{1}{E(\hat{x})A(\hat{x})}d\hat{x}}{\int_0^{L}\frac{1}{E(\hat{x})A(\hat{x})}d\hat{x}}\int_0^{L}\left[\frac{1}{2}\left(\frac{\partial\hat{v}}{\partial\hat{x}}\right)^2+\frac{1}{2}\left(\frac{\partial\hat{w}}{\partial\hat{x}}\right)^2\right]d\hat{x} \quad (15)$$

Substituting $u_{bridge}(\hat{x},\hat{t})$ from Equation (15) into Equations (12) and (13), the governing equations of motion for FG tapered micro-beam take the following forms:

$$\frac{\partial^2}{\partial\hat{x}^2}\left(\left(\mu(\hat{x})A(\hat{x})l(\hat{x})^2+E(\hat{x})I_z(\hat{x})\right)\frac{\partial^2\hat{v}}{\partial\hat{x}^2}\right)+\rho(\hat{x})A(\hat{x})\frac{\partial^2\hat{v}}{\partial\hat{t}^2}-$$
$$\frac{1}{\int_0^{L}\frac{1}{E(\hat{x})A(\hat{x})}d\hat{x}}\left[\int_0^{L}\frac{1}{2}\left(\frac{\partial\hat{v}}{\partial\hat{x}}\right)^2+\frac{1}{2}\left(\frac{\partial\hat{w}}{\partial\hat{x}}\right)^2d\hat{x}\ \right]\frac{\partial^2\hat{v}}{\partial\hat{x}^2}=\hat{f}_y \quad (16)$$

$$\frac{\partial^2}{\partial\hat{x}^2}\left(\left(\mu(\hat{x})A(\hat{x})l(\hat{x})^2+E(\hat{x})I_y(\hat{x})\right)\frac{\partial^2\hat{w}}{\partial\hat{x}^2}\right)+\rho(\hat{x})A(\hat{x})\frac{\partial^2\hat{w}}{\partial\hat{t}^2}-$$
$$\frac{1}{\int_0^{L}\frac{1}{E(\hat{x})A(\hat{x})}d\hat{x}}\left[\int_0^{L}\frac{1}{2}\left(\frac{\partial\hat{v}}{\partial\hat{x}}\right)^2+\frac{1}{2}\left(\frac{\partial\hat{w}}{\partial\hat{x}}\right)^2d\hat{x}\ \right]\frac{\partial^2\hat{w}}{\partial\hat{x}^2}=\hat{f}_z \quad (17)$$

Where $A(\xi)=A_0\xi^2$, $I_y(\xi)=I_{0y}\xi^4$, $I_z(\xi)=I_{0z}\xi^4$. As shown in fig. (2), $\xi=1+(\varepsilon_0-1)x$, ε_0 is the tapered ratio, I_{0y} and I_{0z} are the moments of inertia about y and z axis, respectively, at $\xi=1$. A_0 is also the cross section at $\xi=1$.

Using power-law functions to ensure a smooth distribution of stresses along the longitude direction and all the interfaces, the FG material properties are expected to vary along the axis of the beam as [36]:

$$E(\hat{x}) = E_0 + (E_1 - E_0)(\hat{x}/L)^n, \quad \rho(\hat{x}) = \rho_0 + (\rho_1 - \rho_0)(\hat{x}/L)^n$$
$$\nu(\hat{x}) = \nu_0 + (\nu_1 - \nu_0)(\hat{x}/L)^n, \quad l(\hat{x}) = l_0 + (l_1 - l_0)(\hat{x}/L)^n \tag{18}$$
$$\mu(\hat{x}) = \frac{\mathrm{E}_0 + (E_1 - E_0)(\hat{x}/L)^n}{2\left(1 + \nu_0 + (\nu_1 - \nu_0)\hat{x}/L^n\right)}$$

Where n is the power index parameter, ν_0 and ν_1 are the poisson's ratios, the Indices $'_0'$ and $'_1'$ represent the material type at $x = 0$ and $x = 1$ of the micro-beam respectively.

Utilizing the following dimensionless parameters

$$t = \frac{\hat{t}}{\chi} \quad \chi^2 = \frac{\rho_0 A_0 L^4}{E_0 I_{oy}}, \quad x = \frac{\hat{x}}{L}, \quad w = \frac{\hat{w}}{L}, \quad v = \frac{\hat{v}}{L},$$
$$f_y = \frac{\hat{f_y} L^3}{E_0 I_{oy}}, \quad f_z = \frac{\hat{f_z} L^3}{E_0 I_{oy}}, \quad b = \frac{\hat{b}}{L}, \quad h = \frac{\hat{h}}{L} \tag{19}$$

In which $\hat{h}$ and $\hat{b}$ are thickness and width of the cross section of the micro-bridge, respectively, as shown in fig.(2). The dimensionless equations of motion are derived as:

$$\alpha_y(x)\omega^2 \frac{\partial^2 v}{\partial t^2} + \left(\gamma_{y_2}(x) - \gamma_{y_1}\right)\frac{\partial^2 v}{\partial x^2} + \gamma_{y_3}(x)\frac{\partial^3 v}{\partial x^3} + \gamma_{y_4}(x)\frac{\partial^4 v}{\partial x^4} = f_y \tag{20}$$

$$\alpha_z(x)\frac{\partial^2 W}{\partial t^2} + \left(\gamma_{z_2}(x) - \gamma_{z_1}\right)\frac{\partial^2 W}{\partial x^2} + \gamma_{z_3}(x)\frac{\partial^3 W}{\partial x^3} + \gamma_{z_4}(x)\frac{\partial^4 W}{\partial x^4} = f_z \tag{21}$$

where:

$$\begin{cases} \gamma_{y_1} = \dfrac{L^2}{E_0 I_{0y}} \dfrac{\int_0^1 \frac{1}{2}\left(\frac{\partial v}{\partial x}\right)^2 + \frac{1}{2}\left(\frac{\partial w}{\partial x}\right)^2 dx}{\int_0^1 \frac{1}{E(x)A(x)} dx}, \gamma_{y_2}(x) = \dfrac{\partial^2\left(\mu(x)A(x)l^2(x) + E(x)I_z(x)\right)}{E_0 I_{0y}\partial x^2} \\ \gamma_{y_3}(x) = 2\dfrac{\partial}{E_0 I_{0y}\partial x}\left(\mu(x)A(x)l^2(x) + E(x)I_z(x)\right) \\ \gamma_{y_4}(x) = \dfrac{\mu(x)A(x)l^2(x)}{E_0 I_{0y}} + \dfrac{E(x)I_z(x)}{E_0 I_{0y}}, \alpha_y(x) = \dfrac{\rho(x)A(x)}{\rho_0 A_0} \end{cases} \tag{22}$$

$$\begin{cases} \alpha_z(x) = \alpha_y(x), \gamma_{z_1} = \gamma_{y_1}, \gamma_{z_4}(x) = \dfrac{\mu(x)A(x)l(x)^2}{E_0 I_{0y}} + \dfrac{E(x)I_y(x)}{E_0 I_{0y}} \\ \gamma_{z_2}(x) = \dfrac{\partial^2\left(\mu(x)A(x)l^2(x) + E(x)I_y(x)\right)}{E_0 I_{0y}\partial x^2}, \gamma_{z_3}(x) = 2\dfrac{\partial\left(\mu(x)A(x)l(x)^2 + E(x)I_y(x)\right)}{E_0 I_{0y}\partial x} \end{cases} \tag{23}$$

In this paper, a single pre-assumed mode approach is considered to discretize Equations (20) and (21). Assuming the deflections v and w as

$$\begin{cases} v(x) = q_y(t)\phi_y(x) \\ w(x) = q_z(t)\phi_z(x) \end{cases} \tag{24}$$

where $\phi_y(x)$ and $\phi_z(x)$ are the normalized, self-similar (i.e. independent of the motion amplitude) assumed mode shapes of the beam in y and z directions, respectively. Accordingly, $q_y(t)$ and $q_z(t)$ are the generalized coordinates of the assumed deflection modes $\phi_y(x)$ and $\phi_z(x)$, respectively. Applying the Galerkin decomposition method, the weak forms of Equations (20), (21) are constructed in the forms of:

$$\ddot{q}_y + \zeta_y q_y + \beta_y q_y (q_y^2 + \kappa q_z^2) = F_y \tag{25}$$

$$\ddot{q}_z + \zeta_z q_z + \beta_z q_z (q_z^2 / \kappa + q_y^2) = F_z \tag{26}$$

Where:

$$\begin{cases} \lambda_y = \int_0^1 \frac{\rho A}{\rho_0 A_0} \phi_y^2 dx \qquad F_y = \frac{1}{\lambda_y} \int_0^1 f_y \phi_y dx \\ \zeta_y = \frac{1}{\lambda_y} \int_0^1 \frac{1}{E_0 I_{0y}} \frac{\partial^2}{\partial x^2} \left(\left(\mu A l^2 + E I_z \right) \frac{\partial^2 \phi_y}{\partial x^2} \right) \phi_y dx \end{cases} \tag{27}$$

$$\begin{cases} \lambda_z = \int_0^1 \frac{\rho A}{\rho_0 A_0} \phi_z^2 dx \qquad F_z = \frac{1}{\lambda_z} \int_0^1 f_z \phi_z dx \\ \zeta_z = \frac{1}{\lambda_z} \int_0^1 \frac{1}{E_0 I_{0y}} \frac{\partial^2}{\partial x^2} \left(\left(\mu A l^2 + E I_z \right) \frac{\partial^2 \phi_z}{\partial \hat{x}^2} \right) \phi_z dx \end{cases} \tag{28}$$

$$\begin{cases} \beta_y = -\frac{EA}{2\lambda_y E_0 I_{0y}} \int_0^1 L^2 \frac{\partial^2 \phi_y}{\partial x^2} \phi_y dx . \left(\frac{\partial \phi_y}{\partial x} \right)^2 \Bigg|_{x=1}, \quad \kappa = \frac{\left(\frac{\partial \phi_z}{\partial x} \right)^2}{\left(\frac{\partial \phi_y}{\partial x} \right)^2} \Bigg|_{x=1} \\ \beta_z = -\frac{EA}{2\lambda_z E_0 I_{0y}} \int_0^1 L^2 \frac{\partial^2 \phi_z}{\partial x^2} \phi_z dx . \left(\frac{\partial \phi_z}{\partial x} \right)^2 \Bigg|_{x=1} \end{cases} \tag{29}$$

'.' represents derivative with respect to t. In this work $\phi_y(x)$ and $\phi_z(x)$ for a double tapered micro-bridge are defined as the following form [34, 35]:

$$\phi_{z \text{ or } y}(\xi) = \xi^{-1} [C_1 J_2(Z) + C_2 Y_2(Z) + C_3 I_2(Z) + C_4 K_2(Z)] \tag{30}$$

where $Z = 2\Lambda\xi^{1/2}$, and the values of Λ for different tapered ratios are given in Table (1). *J* and *Y* are Bessel functions of the first and second kind, respectively, and I and K are modified Bessel functions of the first and second kind, respectively. Arbitrary constants $C_1 - C_4$ are calculated through applying the following boundary conditions in $\hat{y}$ and $\hat{z}$ directions respectively:

$$\phi_{\mathrm{z\,or\,y}}(\varepsilon_0) = 0, \quad \frac{\phi_{\mathrm{z\,or\,y}}(\varepsilon_0)}{\partial\xi} = 0, \quad \phi_{\mathrm{z\,or\,y}}(1) = 0, \quad \frac{\partial\phi_{\mathrm{z\,or\,y}}(1)}{\partial\xi} = 0 \tag{31}$$

It should be noted that by assuming identical mode shapes for both lateral directions the parameter κ becomes equal to unity. Equations (25) and (26) represent the weak form of the equations, governing the motion of a micro-beam, which are modeled based on the proposed assumptions and the modified couple stress theory. In the following sections, analytical and numerical solutions, reflecting the static and dynamic performances of the FG tapered micro-beam will be investigated.

3 Static deflection analysis

In this section, by neglecting the inertia terms from Equations (25) and (26) and the coupled nonlinear static deflections of the FG tapered micro-beam under lateral distributed force are investigated. The simplified equations for the static analysis are expressed as:

$$\begin{cases} \zeta_y q_y + \beta_y q_v \left(\mathrm{q}_y^2 + \kappa q_z^2\right) = F_y \\ \zeta_z q_z + \beta_z q_z \left(\mathrm{q}_z^2 / \kappa + q_y^2\right) = F_z \end{cases} \tag{32}$$

As it can be seen, there are two algebraic coupled nonlinear equations, governing the static motions in the transvers directions. A numeric iterative method is utilized to solve simultaneously the above mentioned equations. This iterative procedure is continued until the desired convergence is met.

4 Free vibration analysis

In the next section, the approximate analytical solution according to Homotopy Analysis Method (HAM) is employed to arrive at an analytical solution for non-linear equations of (25) and (26) reflecting the dynamic behavior of the represented model. HAM is an approximate analytic technique for solving nonlinear differential equations. In the following section a brief description for this method is given.

4.1 Homotopy analysis method

To demonstrate the main idea of HAM, consider the general non-linear problem as

$$N[q(\tau)] = 0 \tag{33}$$

In which N represents a general non-linear differential operator and q is considered as an unknown function, describing the exact solution to the non-linear equation. according to Liao, (2004) [37], the Homotopy function is constructed as:

$$N[\psi(\tau,r), u_0(\tau), H(\tau), \hbar, \mathrm{r}] = (1-r)\{\mathrm{L}[\psi(\tau,r) - u_0(\tau)] - r\hbar H(\tau) N[\psi(\tau,r)]\} \tag{34}$$

where $\psi(\tau,\mathrm{r})$ is the primary asymptotic solution, $\hbar$ an auxiliary parameter, $H(\tau) \neq 0$ an auxiliary function, r an embedding parameter, $r \in [0,1]$, L an auxiliary linear operator, and q_0 is an initial guess

of the exact solution q. The convergence condition highly depends on our choices of initial guess, auxiliary linear operator, the nonzero auxiliary parameter and the auxiliary function.

The zero order deformation equation (Homotopy equation) is defined when the Homotopy function is set to zero which lead us to a family of equations, a general form of our original nonlinear equation.

$$(1-\mathrm{r})\{\mathrm{L}[\psi(\tau,\mathrm{r})-q_0(\tau)]\}=r\,\hbar H(\tau)N[\psi(\tau,\mathrm{r})] \tag{35}$$

Now setting $r=0$, and $r=1$, the zero-order equation reduces to Equations (36) and (37), respectively:

$$L[\psi(\tau,0)-q_0(\tau)]=0\rightarrow\psi(\tau,0)=q_0(\tau) \tag{36}$$

$$N[\psi(\tau,1)]=0\rightarrow\psi(\tau,1)=q(\tau) \tag{37}$$

It is obvious that varying the embedding parameter from 0 to 1, the primary solution approaches from the initial guess to the exact solution q. Thus, the following form can be considered for the m th order derivative of q:

$$\mathrm{q}_m(\tau)=\sum_{m=1}^{\infty}\frac{1}{m!}\frac{\partial^m\psi(\tau,\mathrm{r})}{\partial\,\mathrm{r}^m}\bigg|_{r=0} \tag{38}$$

Employing Taylor's series, the expanded forms of $\phi(\tau,\mathrm{r})$ and $\omega(\mathrm{r})$ could be written as:

$$\psi(\tau,\mathrm{r})=\psi(\tau,0)+\sum_{m=1}^{\infty}\frac{1}{m!}\frac{\partial^m\psi(\tau,\mathrm{r})}{\partial\,\mathrm{r}^m}\bigg|_{r=0}r^m=\psi(\tau,0)+\sum_{m=1}^{\infty}q_m(\tau)\mathrm{r}^m \tag{39}$$

$$\omega(\mathrm{r})=\omega_0+\sum_{m=1}^{\infty}\frac{1}{m!}\frac{\partial^m\omega(\mathrm{r})}{\partial\,\mathrm{r}^m}\bigg|_{r=0}\mathrm{r}^m=\omega_0+\sum_{m=1}^{\infty}\omega_m\,\mathrm{r}^m \tag{40}$$

With $q_m(0)=0$ and $\dot{q}_m(0)=0$. In light of (37) and (39) we have:

$$q(\tau)=q_0(\tau)+\sum_{m=1}^{\infty}q_m(\tau) \tag{41}$$

Now in order to estimate $q_m(\tau)$, one must identify the higher order deformation equation. To do so, Equation (35) is differentiated with respect to *r* and the setting *r = 0* and dividing the whole term by $m!$, the higher order deformation equation for *q* is structured in the form:

$$L[q_m(\tau)]=Y_m L[q_{m-1}(\tau)]+\hbar H(\tau)R_m[q_1,...,q_{m-1},\omega_0,...,\omega_{m-1}],\quad \mathrm{Y}_m=\begin{cases}0 & m\le 1\\ 1 & m>1\end{cases} \tag{42}$$

where:

$$R_m[q_1,...,q_{m-1},\omega_0,...,\omega_{m-1}]=\frac{1}{(m-1)!}\frac{\partial^{m-1}N[\psi(\tau,\mathrm{r}),\omega(\mathrm{r})]}{\partial\,\mathrm{r}^{m-1}}\bigg|_{r=0} \tag{43}$$

Since the right hand side of Equation (41) is only dependent on $\{q_1(\tau),q_2(\tau),...,q_{m-1}(\tau)\}$, the m th-order approximation of $q(\tau)$ can be represented by:

$$q(\tau) \approx \sum_{i=0}^{m} q_i(\tau) \tag{44}$$

The corresponding [m, s] pade-approximate about the embedding parameter r, for the series of Equations (39) was proposed by Liao (2004) [37] as a technique to accelerate the convergence of a solution series. Thus, the series of Equations (51) can be expresses in:

$$\psi(\tau, r) = \psi(\tau, 0) + \sum_{m=1}^{\infty} q_m(\tau) \mathrm{r}^m = \frac{\sum_{k=0}^{m} A_{m,k}(\tau) \mathrm{r}^k}{\sum_{k=0}^{n} B_{\mathrm{s},k}(\tau) \mathrm{r}^k} \tag{45}$$

In which, $A_{m,k}$ and $B_{\mathrm{s},k}$ are computed by the following set of approximations:

$$\{q_0(\tau), q_1(\tau), q_2(\tau), ..., q_{m+s}(\tau)\} \tag{46}$$

Now, if $r = 1$, the $[m, \mathrm{s}]$ Homotopy pade approximant is constructed as:

$$\phi(\tau, 1) = \frac{\sum_{k=0}^{m} A_{m,k}(\tau)}{\sum_{k=0}^{n} B_{\mathrm{s},k}(\tau)} \tag{47}$$

4.2 Application of Homotopy Pad'e method to the problem

According to Equations (25) and (26), eliminating the external forces, we have:

$$N_y = \omega_y{}^2 \frac{\partial^2 q_y}{\partial \tau_y{}^2} + \zeta_y q_y + \beta_y \mathrm{q}_y \left(q_y^2 + \kappa q_z^2\right) \tag{48}$$

$$N_z = \omega_z{}^2 \frac{\partial^2 q_z}{\partial \tau_z{}^2} + \zeta_z q_z + \beta_z \mathrm{q}_z \left(q_z^2 / \kappa + q_y^2\right) \tag{49}$$

$$L_y[q(\tau_y, \mathrm{r})] = \omega_{y0}^2 \left(\frac{\partial^2 q_y(\tau_y, \mathrm{r})}{\partial \tau_y{}^2} + q_y(\tau_y, \mathrm{r}) \right) \tag{50}$$

$$L_z[q(\tau_z, \mathrm{r})] = \omega_{z0}^2 \left(\frac{\partial^2 q_z(\tau_z, \mathrm{r})}{\partial \tau_z{}^2} + q_z(\tau_z, \mathrm{r}) \right) \tag{51}$$

in which $\tau_y = \omega_y t$, $\tau_z = \omega_z t$ .By considering:

$$\begin{cases} u_{y,0} = a_y .cos(\tau_y) \\ u_{z,0} = a_z .cos(\tau_z) \end{cases} \tag{52}$$

where a_y and a_z are vibration's amplitude in y and z directions, respectively, According to Equation (43) with $H(\tau) = 1, \hbar = -1$ and for $m = 1$, we may write:

$$R_{y,m}=R_{y,1}=\left(-\omega_{y,(m-1)}^2 a_y+\zeta_y a_y+\frac{3}{4}\beta_y a_y^3+\frac{1}{2}\kappa\beta_y a_y a_z^2\right)\cos(\tau_y)+\frac{1}{4}\beta_y a_y^3\cos(3\tau_y)$$
$$+\frac{1}{4}\beta_y\kappa a_y a_z^2\cos(\tau_y-2\tau_z)+\frac{1}{4}\beta_y k a_z^2 a_y\cos(\tau_y+2\tau_z) \quad (53)$$

$$R_{z,m}=R_{z,1}=\left(-\omega_{z,(m-1)}^2 a_z+\zeta_z a_z+\frac{3}{4}\beta_z a_z^3/\kappa+\frac{1}{2}a_z\beta_z a_y^2\right)\cos(\tau_z)+\frac{1}{4}\beta_z a_z^3/\kappa\cos(3\tau_z)$$
$$+\frac{1}{4}\beta_z a_z a_y^2\cos(2\tau_y-\tau_z)+\frac{1}{4}\beta_z a_y^2 a_z\cos(2\tau_y+\tau_z) \quad (54)$$

To avoid the secular terms in the final solution, sum of the coefficients of $\cos(\tau)$ are taken equal to zero, in the case of $\kappa=1$, it is a close approximation to consider $\tau_y=\tau_z=\tau$, so we have:

$$\omega_{y,(m-1)}=\omega_{y,0}=\sqrt{\zeta_y+\frac{3}{4}\beta_y a_y^2+\frac{3}{4}\beta_y a_z^2},\quad \omega_{z,(m-1)}=\omega_{z,0}=\sqrt{\zeta_z+\frac{3}{4}\beta_z a_y^2+\frac{3}{4}\beta_z a_z^2} \quad (55)$$

Solving Equations (42) for $m=1$, $q_{y,1}$ and $q_{z,1}$:

$$q_{y,m}=q_{y,1}=\frac{\left(\left(\beta_y a_y^3+\beta_y a_z^2 a_y\right)\cos(3\tau)-\left(\beta_y a_y^3+\beta_y a_z^2 a_y\right)\cos(\tau)\right)}{24\beta_y a_y^2+24\beta_y a_z^2+32\zeta_y} \quad (56)$$

$$q_{z,m}=q_{z,1}=\frac{\left(\left(\beta_z a_z^3+\beta_z a_y^2 a_z\right)\cos(3\tau)-\left(\beta_z a_z^3+\beta_z a_y^2 a_z\right)\cos(\tau)\right)}{24\beta_z a_z^2+24\beta_z a_y^2+32\zeta_z} \quad (57)$$

Subsequently, for m=2 and calculating the expressions for $R_{y,2}$ and $R_{z,2}$ we arrive at results for $\omega_{y,2}$ and $\omega_{z,2}$. We continue this procedure to higher order level for $m=5$, which an appropriate approximation in consistent with numerical data for natural frequencies of the micro-bridge will be achieved. According to [37] the [1,1] and [2,2] Homotopy- pade approximations for $\omega_{v/w}$ and $q_{v/w}$ are found as:

$$\omega_{y/z,[1,1]}=\frac{\omega_{y/z,0}\left(\omega_{y/z,1}-\omega_{y/z,2}\right)+\omega_{y/z,1}^2}{\omega_{y/z,1}-\omega_{y/z,2}} \quad (58)$$

$$\omega_{y/z,[2,2]}=\frac{\begin{bmatrix}\omega_{y/z,0}\left(\omega_{y/z,2}\left(\omega_{y/z,3}+\omega_{y/z,4}\right)+\omega_{y/z,1}\left(\omega_{y/z,3}-\omega_{y/z,4}\right)\right)\\+\omega_{y/z,1}\omega_{y/z,2}\left(2\omega_{y/z,3}-\omega_{y/z,2}\right)+(\omega_{y/z,3}-\omega_{y/z,4})\omega_{y/z,1}^2\\-\omega_{y/z,2}^3-\omega_{y/z,0}\left(\omega_{y/z,3}^2+\omega_{y/z,2}^2\right)\end{bmatrix}}{\omega_{y/z,4}\omega_{y/z,2}-\omega_{y/z,3}^2-\omega_{y/z,4}\omega_{y/z,1}+\omega_{y/z,2}\omega_{y/z,3}+\omega_{y/z,1}\omega_{y/z,3}-\omega_{y/z,2}^2} \quad (59)$$

$$q_{y/z,[1,1]}=\frac{q_{y/z,0}\left(q_{y/z,1}-q_{y/z,2}\right)+q_{y/z,1}^2}{q_{y/z,1}-q_{y/z,2}} \quad (60)$$

$$q_{y/z,[2,2]} = \frac{\begin{bmatrix} q_{y/z,0}\left(q_{y/z,2}\left(q_{y/z,3}+q_{y/z,4}\right)+q_{y/z,1}\left(q_{y/z,3}-q_{y/z,4}\right)\right) \\ +q_{y/z,1}q_{y/z,2}\left(2q_{y/z,3}-q_{y/z,2}\right)+\left(q_{y/z,3}-q_{y/z,4}\right)q_{y/z,1}^2 \\ -q_{y/z,2}^3-q_{y/z,0}\left(q_{y/z,3}^2+q_{y/z,2}^2\right) \end{bmatrix}}{q_{y/z,4}q_{y/z,2}-q_{y/z,3}^2-\omega_{y/z,4}\omega_{y/z,1}+q_{y/z,2}q_{y/z,3}+q_{y/z,1}q_{y/z,3}-q_{y/z,2}^2} \quad (61)$$

5 Numerical results

In this section, numerical and analytical results are provided in order to investigate the effects of various material and geometrical properties on the static and dynamic responses of doubly clamped FG tapered micro-beam. The obtained results are compared with the corresponding results calculated by the classical beam theory to clarify the distinction that have been made in utilizing the length scale parameter. The micro-beam is composed of aluminum (AL) and silicon-carbide (SiC). The material properties of aluminum are $E_1 = 70\text{GPa}$, $\nu_1 = 0.3$, and $\rho_1 = 2702\,kg/m^3$, and those of silicon carbide are $E_0 = 427\text{GPa}$, $\nu_0 = 0.17$ and $\rho_0 = 3100\,kg/m^3$ [38]. Since each of the participating constituents material has a specific value of the length scale parameter, it is concluded that the material length scale parameter of the micro-bridge varies along the beam axis. In the present work, the material length scale parameter of silicon-carbide are respectively assumed as $l_1 = 10\mu m$ and $l_0 = 5\mu m$. According to Equation (19) the effective material length scale parameter can be estimated.

The dimensionless static deflections in $\hat{z}$ direction for Nonlinear and linear micro-bridge is depicted in Fig. (3). It is clear that adding the distributed force in y direction, reduces the nonlinear static deflection of micro-bridge in z direction. Furthermore considering the nonlinearity will reduce the static deflection. This is due to considering the mid-plane stretching that causes a coupling between equations of both lateral displacements.

Fig. (4) plots the frequency ratio (the ratio of non-classical FG tapered-micro-beam frequency to the Non-FG one) for doubly clamped boundary conditions, for different value of power index parameters.

The key point that can be understood from Fig. (4) is that by increasing the power index parameter, the sensitivity to initial deflection heightens. Table. (2) expresses the nonlinear natural frequencies in z direction for various tapered and slender ratios. Since the coupling term is independent of the dimensionless parameter h/b (the ratio of thickness, the edge that is parallel to z axis to the width, the edge that is parallel to y axis), changing the size of the edge b (width), has a negligible influence on the natural frequency in z direction, thus, the effect of this parameter is not reported in these tables. On the other hand, in table. (3), the corresponding values for natural frequencies in y direction and the effects of changing size of the edge b (changing the h/b parameter) on vibrations along the y axis, can be observed. Numerical results are provided in order to evaluate the accuracy of the analytical HAM method. It should be noted that for a square cross section, the nonlinear natural frequencies are identical for vibrations in both directions, regardless of the given amplitude.

Fig. (5) plot the natural frequency ratio (the ratio of non-classical FG tapered-micro-bridge frequency to the classical one), versus the initial deflection for different values of h/l. It is realized that considering both lateral deflections in calculations the nonlinear natural frequency has a significant effects on dynamic responses.

Due to the mid plane stretching, accounting for the third dimension into the vibration problem, increases the corresponding natural frequencies. The values obtained for 2D analysis also increase as the initial deflection grows. Furthermore, it is illustrated in Fig. (5) that the natural frequency computed by

the proposed model here, is much higher than that predicted by the classical beam theory. Hence, for larger values of h/l (the ratio of thickness to the length scale parameter of the beam), as shown in Fig. (5) the nonlinear responses approaches to the responses of the classical beam theory.

Table. (4) reflects the natural frequency of a micro bridge for a 3D analysis by multiple time scales method (MTS), which are provided by Mojahedi & Rahaeifard (2016) [32] The corresponding results found by Homotopy analysis method as well as the numerical solutions are reported to validate the proposed HAM method in comparison with the MTS 3rd order method. As one may observe, for $a_y > 0.03$, the deviation of Harmonic Balance method results from the numerical ones increases significantly, while the corresponding error associated with HAM results are negligible. As indicated in section1, the results in Table 4. reveal the higher capability of HAM in dealing with large parameters strong nonlinearities and higher vibration amplitude than MTS.

6 Summary and Conclusion

A nonlinear model for doubly clamped tapered FG micro-beams based on modified couple stress, considering the effects of two coupled bending deformations in lateral directions and also mid-plane stretching, was considered here. After constructing the Lagrangian of the motion, applying the Hamilton principle, the nonlinear 3D equations of motion were derived. In this method, a uni-modal approach was employed to discretize the governing equations and the resultant uni-modal differential equations of motion were solved for static and dynamic responses. The deflections of the Single and doubly clamped tapered FG micro-beams under different loading conditions were numerically calculated. The correspondent results showed that considering the lateral loading in one direction reduces the static deflection in other direction. In the case of dynamic analysis, the nonlinear natural frequency for various geometrical and material compositional properties were calculated using analytical Homotopy-pade method. It can be observed that by increasing the amplitude of the vibration, the difference between linear and nonlinear natural frequencies increase, and for higher values of h/l, both values approaches those found through the classical beam theory. Furthermore, it was observed that increasing the power index parameter resulted in higher natural frequency values. The advantage of Homotopy method in terms of computational cost and accuracy over a classic analytical method, MTS method (recently employed in the literature to investigate the 3D vibration of micro beams), in problems with strong nonlinearity and high amplitudes are discussed by a comparison study, which showed the accuracy of the HAM technique. The corresponding non-linear natural frequencies calculated by FFT as a numerical method were reported to certify the proposed HAM method.

Compliance with Ethical Standards

Conflict of Interest: The authors declare that they have no conflict of interest.

References

[1] Lotfi M, Moghimi M. " Transient behavior and dynamic pull-in instability of electrostatically-actuated fluid-conveying microbeams", *International Journal of Microsyst Technologies*, 23(13), pp. 6015–6023 (2017).

[2] Chong, A. C. M, Yang, F., Lam, D. C. C., and Tong, P. 'Torsion and bending of micron-scaled structures', *Journal of Materials Research*, *16*(4), pp. 1052–1058 (2001).

[3] Stölken, J. S., & Evans, A. G. "A microbend test method for measuring the plasticity length scale", *Acta Material*, *46*(14), pp. 5109–5115 (1998).

[4] Q. Ma and D. R. Clarke, "Size dependent hardness of silver single crystals," *J. Mater. Res.*, vol.

10, no. 04, pp. 853–863, 1995.

[5] Chong, Arthur C.M, and Lam, D. C. C. "Strain gradient plasticity effect in indentation hardness of polymers", *Materials Research*, *14*(10), pp. 4103–4110 (1999).

[6] Yang, F., Chong, A. C. M., Lam, D. C. C., and Tong, P. "Couple stress based strain gradient theory for elasticity", *International Journal of Solids and Structures*, *39*(10), pp. 2731–2743 (2002).

[7] Mindlin, R. D. "Second gradient of strain and surface-tension in linear elasticity", *International Journal of Solids and Structures*, *1*(4), pp. 417–438 (1965).

[8] Fleck, N. A., and Hutchinson, J. W. "A phenomenological theory for strain gradient effects in plasticity", *Journal of the Mechanics and Physics of Solids*, *41*(12), pp. 1825–1857 (1993).

[9] Fleck, N. A., and Hutchinson, J. W. "Strain Gradient Plasticity", *Advances in Applied Mechanics*, 33 pp. 295–361, (1997).

[10] Fleck, N. A., & Hutchinson, J. W. "A reformulation of strain gradient plasticity", *Journal of the Mechanics and Physics of Solids*, *49*(10), pp. 2245–2271 (2001).

[11] Ansari, R., Faraji Oskouie, M., and Rouhi, H. "Studying linear and nonlinear vibrations of fractional viscoelastic Timoshenko micro- / nano-beams using the strain gradient theory", *Nonlinear Dynamics*, *87*(1), pp. 695–711 (2016).

[12] Li, X., Li, L., Hu, Y., Ding, Z., and Deng, W. "Bending , buckling and vibration of axially functionally graded beams based on nonlocal strain gradient theory", C*omposite Structures*, 165, pp. 250-265 (2017).

[13] Mindlin, R. D., and Tiersten, H. F. "Effects of couple-stresses in linear elasticity", *Archive for Rational Mechanics and Analysis*, *11*(1), pp. 415–448 (1962).

[14] Jafari-talookolaei, R., Ebrahimzade, N., and Rashidi-juybari, S. "Bending and vibration analysis of delaminated Bernoulli-Euler microbeams using the modi ed couple stress", *Scientia Iranica*, *25*, pp. 675–688. (2018).

[15] Hadi, M., Omid, J., and Mostafa, Z. "Size-Dependent Vibration Analysis of FG Microbeams in Thermal Environment Based on Modified Couple Stress Theory", *Iranian Journal of Science and Technology, Transactions of Mechanical Engineering*, 43, pp. 761–771 (2011).

[16] Bhattacharya, S., & Das, D. "Free vibration analysis of bidirectional-functionally graded and double-tapered rotating micro-beam in thermal environment using modified couple stress theory", *Composite Structures, 215, pp. 471-492* (2019).

[17] Baghani, M. "Analytical study on size-dependent static pull-in voltage of microcantilevers using the modified couple stress theory", *International Journal of Engineering Science*, *54*, pp. 99–105 (2012).

[18] Lü, C. F., Lim, C. W., and Chen, W. Q. "Size-dependent elastic behavior of FGM ultra-thin films based on generalized refined theory", *International Journal of Solids and Structures*, *46*(5), pp.

1176–1185 (2009).

[19] Fu, Y., Du, H., and Zhang, S. "Functionally graded TiN/TiNi shape memory alloy films", *Materials Letters*, *57*(20), pp. 2995–2999 (2003).

[20] Rahaeifard, M., Kahrobaiyan, M. H., and Ahmadian, M. T. "Sensitivity analysis of atomic force microscope cantilever made of functionally graded materials", *ASME 2009 International Design Engineering Technical Conferences and Computers and Information in Engineering Conference*, pp 539–544 (2009).

[21] Bashirpour, M., Forouzmehr, M., and Hosseininejad, S. E. "Improvement of Terahertz Photoconductive Antenna using Optical Antenna Array of ZnO Nanorods", *Scientific Reports*, pp. 1–8 (2019).

[22] Baghani, M., & Fereidoonnezhad, B. "Limit analysis of FGM circular plates subjected to arbitrary rotational symmetric loads using von-Mises yield criterion", *Acta Mechanica*, *224*(8), pp. 1601–1608 (2013).

[23] Baghani, M, Mazaheri, H., and Salarieh, H. "Analysis of large amplitude free vibrations of clamped tapered beams on a nonlinear elastic foundation", *Applied Mathematical Modelling*, *38*(3), pp. 1176–1186 (2014).

[24] Sadeghi, H., Baghani, M., and Naghdabadi, R. "Strain Gradient Elasticity Solution for Functionally Graded Micro", *International Journal of Engineering Science*, *50*(1), pp. 20–23 (2011).

[25] Bashirpour, M., Kefayati, A., Kolahdouz, M., & Aghababa, H. "Tuning the Electronic Properties of Symetrical and Asymetrical Boron Nitride Passivated Graphene Nanoribbons : Density Function Theory", *Journal of Nano Research*, *54*, pp. 35–41 (2018).

[26] Baghani, M, Mazaheri, H., & Salarieh, H. "Analysis of large amplitude free vibrations of clamped tapered beams on a nonlinear elastic foundation", *Applied Mathematical Modelling*, *38*(3), pp. 1176–1186 (2014).

[27] Raju, S. S., Umapathy, M., and Uma, G. "High-output piezoelectric energy harvester using tapered beam with cavity", *Journal of Intelligent Material Systems and Structures*, 29(5), pp. 1–16 (2017).

[28] Mohammadsalehi, M., Zargar, M., and Baghani, M. "Study of non-uniform viscoelastic nanoplates vibration based on nonlocal first-order shear deformation theory. *Meccanica*, *52*(4–5), pp. 1063–1077 (2017).

[29] Zhao, X. W., Hu, Z. D., and Heijden, G. H. M. Van Der. "Dynamic analysis of a tapered cantilever beam under a travelling mass. *Meccanica*, *50*(6), pp. 1419–1429 (2015).

[30] Mojahedi, M., Ahmadian, M. T., and Firoozbaksh, K. "Effects of Casimir and Van Der Waals Forces on the Pull-in Instability of the Nonlinear Micro and Nano-Bridge Gyroscopes", *International Journal of Structural Stability and Dynamics*, *14*(02), pp. 135–159 (2014).

[31] Mojahedi, M., Ahmadian, M. T., And Firoozbakhsh, K. "The influence of the intermolecular surface forces on the static deflection and pull-in instability of the micro/nano cantilever gyroscopes", *Composites Part B: Engineering*, *56*, pp. 336–343 (2014).

[32] Mojahedi, M., and Rahaeifard, M. "A size-dependent model for coupled 3D deformations of nonlinear microbridges", *International Journal of Engineering Science*, *100*, pp. 171–182 (2016).

[33] Park, S. K., and Gao, X. "Bernoulli–Euler beam model based on a modified couple stress theory", *IOP science, 2355*, pp. 0–5 (2006)

[34] Liao, S. *Homotopy Analysis Method in Nonlinear Differential Equations*, (2011).
.
[35] Carrera, E., Giunta, G., and Petrolo, M. *Beam Structures, Beam Structures: Classical and Advanced Theories*, *John Wiley & Sons* (2011).

[36] Baghani, Mostafa, MohammadSalehi, M., and Dabaghian, P. H. "Analytical couple-stress solution for size-dependent large-amplitude vibrations of FG tapered-nanobeams", *Latin American Journal of Solids and Structures*, *13*(1), pp. 95–118 (2014).

[37] Liao, S. *Beyond Perturbation: An introduction to the Homotopy analysis method*, *CHAPMAN & HALL/CRC* , (2004)..

[38] Zhang, B., He, Y., Liu, D., Gan, Z., and Shen, L. "Size-dependent functionally graded beam model based on an improved third-order shear deformation theory" *European Journal of Mechanics, A/Solids*, *47*, pp. 211–230 (2014).

Shadi Haddad obtained her B.S. degree in Mechanical Engineering from Shahid Chamran University Ahvaz, Iran, in 2015, and his M.S. degree in Mechanical Engineering from the Department of Mechanical Engineering at Tehran University, Tehran, Iran, in 2018. Her research interests include vibration analysis, system dynamics and controls, fault detection, micro-electromechanical systems.

Mostafa Baghani received his BS degree in Mechanical Engineering from University of Tehran, Iran,. in 2006 and his MS and PhD degrees in Mechanical Engineering from the Department of Mechanical Engineering at Sharif University of Technology, Tehran, Iran, in 2008 and 2012, respectively. He is now an Assistant Professor in the School of Mechanical Engineering, University of Tehran. His research interests include solid mechanics, nonlinear finite element method, and shape-memory materials constitutive modeling.

Mohammad Reza Zakerzadeh received his B.S. Degree, M.S. Degree and his Ph.D. Degree all in mechanical engineering from Sharif University of Technology, Tehran, Iran, in 2002, 2005 and 2012 respectively. Since 2012 he has been with the School of mechanical Engineering, College of Engineering of University of Tehran. He is now Associate Professor and his research activities include smart material and structures, Shape Memory Alloy (SMA), dynamics, control and robotics.

Figures and Tables Caption:

Fig.1 A schematic view of micro-bridge under distributed forces in lateral directions.

Fig 2. Initial configuration of the tapered micro-bridge.

Fig. 3. Static deflection along the x axis. FG double tapered micro-bridge $\varepsilon_0 = 0.04,\ L/h = 20,\ h/l = 3,\ h = b,\ n = 2$

Fig 4. Natural frequency ratio versus initial deflection for different power index parameters. FG micro-bridge, $\omega_c = 15.119$.

Fig. 5. Natural frequency ratio versus initial deflection for different ratios of h/l. FG micro-bridge, $\omega_{cl} = 13.199$, $\varepsilon_0 = 0.04,\ L/h = 20,,\ h/b = 1, n = 2$ and ω_{cl} is the classical natural frequency.

Table 1. Values of parameter Λ for different tapered ratios.

Table. 2. Nonlinear natural frequency ($\omega_z \times \sqrt{\rho_0 A_0 L^4 / E_0 I_{oy}}$) for a FG micro-bridge and comparison between the present research and numerical FFT results. Relative differences are concluded for each case $\varepsilon_0 = 0.4,\ \mathrm{L/h} = 20,\ \mathrm{a}_y = \mathrm{a}_z = .03,\ n = 2,\ \mathrm{h/l} = 3$

Table. 3. Nonlinear natural frequency ($\omega_z \times \sqrt{\rho_0 A_0 L^4 / E_0 I_{oy}}$) for a FG micro-bridge and comparison between the present research and numerical FFT results. Relative differences are concluded for each case $\varepsilon_0 = 0.4,\ \mathrm{L/h} = 20,\ \mathrm{a}_y = a_z = 0.03,\ n = 2,\ \mathrm{h/l} = 3$

Table. 4. Comparison between the present research (HAM) and (MTS) method and numerical FFT results in calculating the Nonlinear natural frequency ($\omega_z \times \sqrt{\rho A L^4 / EI}$) corresponding to a 3D analysis. Relative differences are concluded for each case. In this calculations we have: $\varepsilon_0 = 1,\ \mathrm{L/h} = 30,\ n = 0,\ \mathrm{h/l} = 3$, $\mu = 61GPa,\ E = 150GPa,\ \rho = 2300kg/m^3,\ \nu = 0.25,\ h = b$

Figures

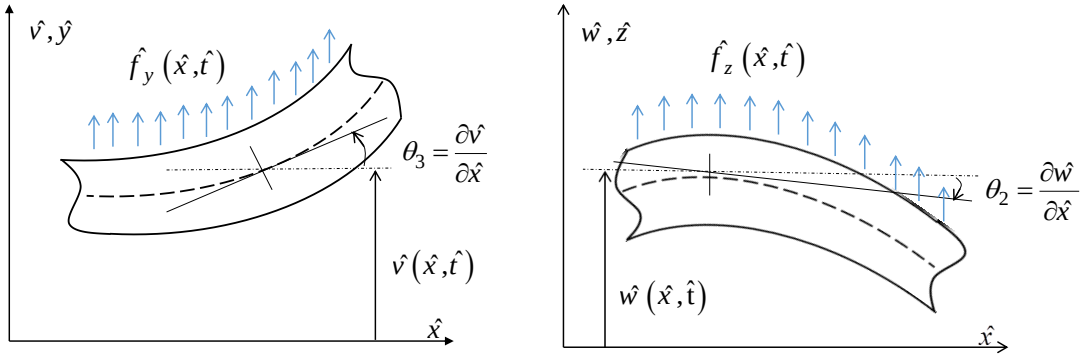

Fig.1 A schematic view of micro-bridge under distributed forces in lateral directions.

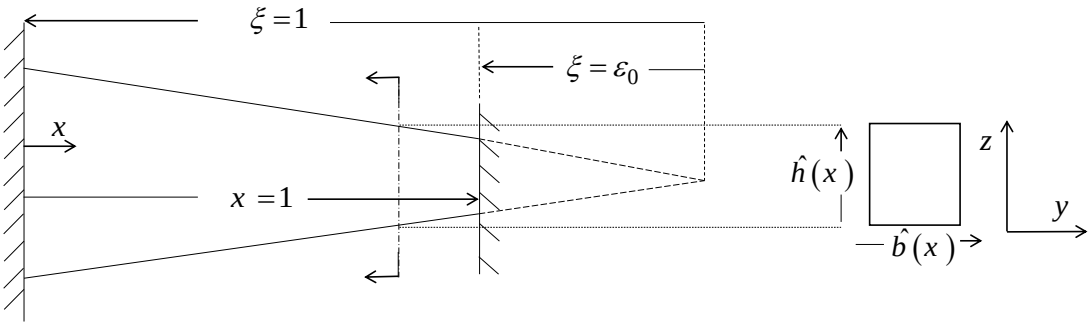

Fig 2. Initial configuration of the tapered micro-bridge

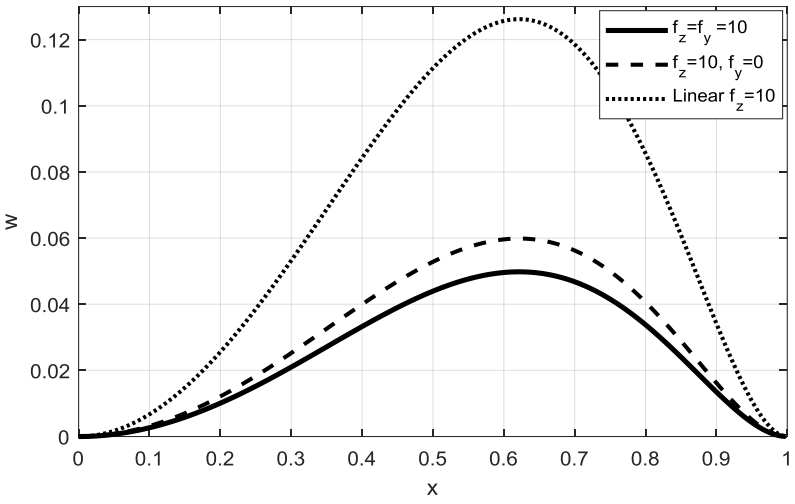

Fig. 3. Static deflection along the x axis. FG double tapered micro-bridge $\varepsilon_0 = 0.04,\ L/h = 20,\ h/l = 3,\ h = b,\ n = 2$

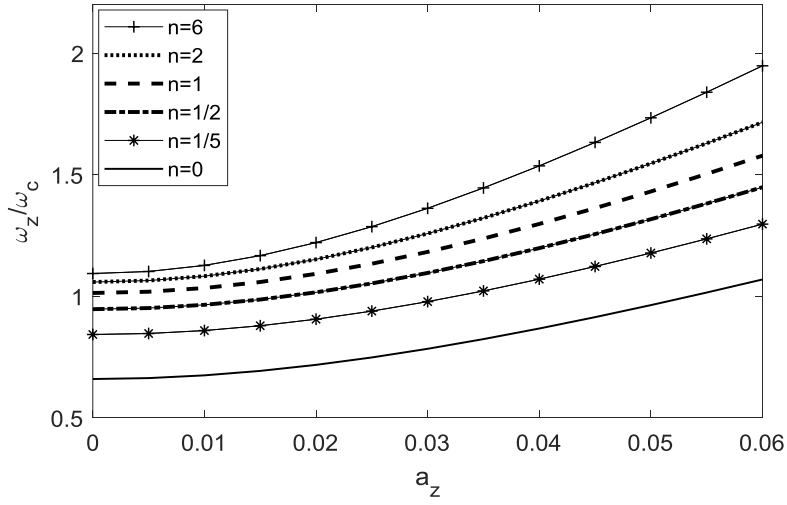

Fig 4. Natural frequency ratio versus initial deflection for different power index parameters. FG micro-bridge, $\omega_c = 15.119$.

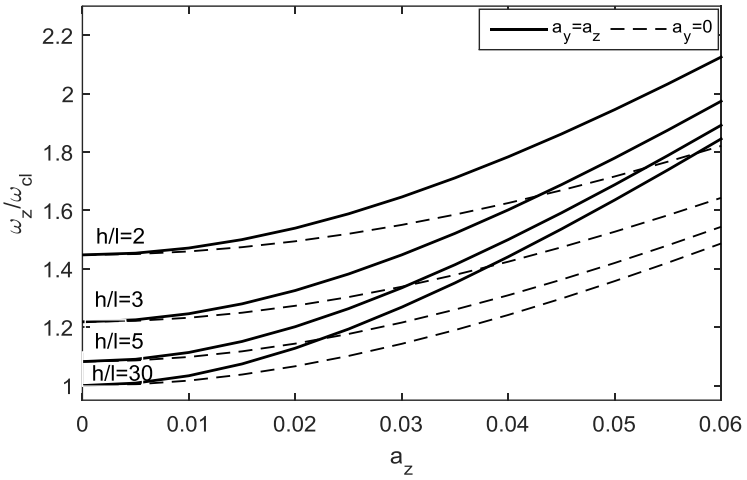

Fig. 5. Natural frequency ratio versus initial deflection for different ratios of h/l . FG micro-bridge, $\omega_{cl}=13.199$, $\varepsilon_0=0.04,\ L/h=20,,\ h/b=1, n=2$ and ω_{cl} is the classical natural frequency.

Table 1. Values of parameter Λ for different tapered ratios

	ε_0	0.2	0.4	0.6	0.8
Λ	Doubly clamped tapered micro-beam	4.398	6.495	10.524	22.415

Table. 2. Nonlinear natural frequency ($\omega_z \times \sqrt{\rho_0 A_0 L^4 / E_0 I_{oy}}$) for a FG micro-bridge and comparison between the present research and numerical FFT results. Relative differences are concluded for each case $\varepsilon_0=0.4,\ \mathrm{L/h}=20,\ \mathrm{a}_y=\mathrm{a}_z=.03,\ n=2,\ \mathrm{h/l}=3$

	$L/h=10$		$L/h=15$		$L/h=20$		$L/h=25$	
$\epsilon*$	HAM	FFT	HAM	FFT	HAM	FFT	HAM	FFT
	Relative error %		Relative error %		Relative error %		Relative error %	
0.2	16.139	16.297	17.266	17.396	18.720	18.868	20.427	20.647
	0.971		0.749		0.783		1.068	
.04	16.897	16.886	17.856	17.945	19.111	19.262	20.604	20.919
	0.064		0.496		0.786		1.507	
0.6	18.348	18.358	19.250	19.323*	20.439	20.556	21.865	21.970
	0.057		0.380		0.573		0.480	
0.8	19.929	19.831	20.798	20.859*	23.340	23.561	23.344	23.422
	0.493		0.294		0.942		0.336	

Table. 3. Nonlinear natural frequency ($\omega_y \times \sqrt{\rho_0 A_0 L^4 / E_0 I_{oz}}$) for a FG micro-bridge and comparison between the present research and numerical FFT results. Relative differences are concluded for each case $\varepsilon_0 = 0.4$, L/ h = 20, $a_y = a_z = 0.03$, $n = 2$, h/ l = 3

		$L/h = 10$		$L/h = 15$		$L/h = 20$		$L/h = 25$	
$\epsilon*$	h/b	HAM	FFT	HAM	FFT	HAM	FFT	HAM	FFT
		Relative error %		Relative error %		Relative error %		Relative error %	
0.2	2	13.060	12.956	14.427	14.269	16.135	16.219	18.085	18.221
		0.803		1.106		0.520		0.747	
	3	12.406	12.133	13.837	13.750	15.609	15.785	17.617	17.625
		2.251		0.631		1.112		0.048	
	5	12.057	11.804	13.525	13.505	15.333	15.462	17.372	17.342
		2.141		0.005		0.836		0.175	
0.4	2	12.468	12.224	13.738	13.689	15.329	15.395	17.149	16.422
		1.996		0.357		0.429		4.423	
	3	11.461	11.213	12.830	12.668	14.520	14.597	16.428	17.285
		2.206		1.277		0.528		4.958	
	5	10.909	10.703	12.339	12.144	14.087	14.101	16.047	16.292
		1.922		1.599		0.101		1.505	
0.6	2	12.783	12.625	14.044	13.905	15.629	15.739	17.447	16.695
		1.248		0.997		0.701		4.499	
	3	11.459	11.270	12.850	12.536	14.564	14.545	16.498	15.697
		1.675		2.503		0.127		5.104	
	5	9.534	9.308	11.164	10.824	13.098	13.006	15.217	14.823
		2.422		3.134		0.705		2.658	
0.8	2	13.332	13.169	14.597	14.334	16.192	16.192	18.028	17.261
		1.238		1.831		0.0		4.441	
	3	11.708	11.503	13.129	12.846	14.881	14.774	16.858	16.032
		1.774		2.203		0.722		5.148	
	5	10.783	10.574	12.309	11.999	14.162	14.024	16.226	15.356
		1.976		2.578		0.979		5.662	

Table. 4. Comparison between the present research (HAM) and (MTS) method and numerical FFT results in calculating the Nonlinear natural frequency ($\omega_z \times \sqrt{\rho A L^4 / EI}$) corresponding to a 3D analysis. Relative differences are concluded for each case. In this calculations we have: $\varepsilon_0 = 1$, L/ h = 30, $n = 0$, h/ l = 3 , $\mu = 61GPa$, $E = 150GPa$, $\rho = 2300kg/m^3$, $\nu = 0.25$, $h = b$

$a_y = a_z$	0.01	0.02	0.03	0.04	0.05	0.06
FFT	29.919	35.620	43.001	51.821	61.312	70.630
HAM	29.897	35.509	42.584	51.519	61.113	70.914
HAM Relative error %	0.073%	0.312%	0.970%	0.583%	0.325%	0.402%
MTS	28.658	31.283	35.656	41.779	49.652	59.273
MTS Relative error%	4.215%	12.176%	17.081%	19.378%	19.017%	25.990%